Materials for Renewable and Sustainable Energy (2019) 8:10
https://doi.org/10.1007/s40243-019-0147-y

ORIGINAL PAPER

Robust electrochemistry of black TiO_2 as stable and high-rate negative electrode for lithium-ion batteries

Shivaraj B. Patil[1] · Harish Phattepur[2] · Brij Kishore[3] · R. Viswanatha[4] · G. Nagaraju[1]

Received: 3 March 2019 / Accepted: 24 June 2019 / Published online: 10 July 2019

Abstract

Electrochemically stable black TiO_2 composed of Ti^{3+} ions and oxygen vacancies is successfully synthesized by a facile and economic sol–gel method followed by calcination in nitrogen atmosphere at 400 °C for 2 h. Several physicochemical techniques are probed to validate the desired state of the obtained material. The material is formed in a pure state with an average size of 10 nm. The electrochemical studies are conducted for its use as negative electrode for Li-ion batteries. At high current rate of 5 C, the electrodes deliver a high discharge capacity of 226 mA h g^{-1} even after 150 cycles. Similarly, the electrodes also deliver discharge capacities of 197 and 153 mA h g^{-1} at current rates of 7 C and 10 C, respectively. The robust electrochemical properties of black TiO_2 including large specific capacities at high current rates and high stability are ascribed to the formation of defective structure, conductive Ti^{3+} ions and oxygen vacancies.

Keywords Black TiO_2 · High-rate negative electrode · Lithium-ion battery · Ti^{3+} ions

Introduction

Low cost and high safety along with large specific capacity are the critical factors for choosing materials as an electrode (cathode or anode) for lithium-ion batteries (LIBs). Hence, it is important to develop a high specific capacity material along with low cost and high safety. It is often observed that materials with high theoretical capacity suffer from low cycling stability [1–4]. TiO_2 (white) is well established as a low-cost material with high safety. The remarkable electrochemical cycling stability of TiO_2 makes it more attractive for LIBs. TiO_2 is also documented as high-rate anode which operates within the potential window of the most common electrolytes, thus inhibiting the formation of solid–electrolyte interface (SEI) and related gas emission associated with electrolyte decomposition [5, 6].

A limiting factor to its implementation and application would be the high operating potential that makes the energy density of Li-ion battery based on TiO_2 negative electrode lower than that featuring graphite anode. Apart from low theoretical specific capacity, it also suffers from high intrinsic resistance (evident from its wide bandgap of 3.2 eV), structural distortion (during Li^+ de-/intercalation) and most importantly, formation of passive oxidation layer on the surface when it is annealed in air atmosphere which hinders the kinetics of the Li^+ ions [7–9].

Many efforts have been made to tackle these shortcomings. Different polymorphs like anatase [10], brookite [5], rutile [11], extensive amorphous TiO_2 [12] have been introduced to enhance the electrochemical performance. The research is also focused on synthesizing TiO_2 with different morphologies such as nanoparticles (NPs), nanorods (NRs), etc., to improve its electrochemical performance [6, 13, 14]. Recently, black TiO_2 nanoparticles (B-TiO_2 NPs) have been explored as a solution [8, 9]. B-TiO_2 demonstrates narrowed

Electronic supplementary material The online version of this article (https://doi.org/10.1007/s40243-019-0147-y) contains supplementary material, which is available to authorized users.

✉ G. Nagaraju
nagarajugn@rediffmail.com

1 Energy Materials Research Laboratory, Department of Chemistry, Siddaganga Institute of Technology (Affiliated to Visvesvaraya Technological University, Belagavi), Tumakuru 572103, India

2 Department of Chemical Engineering, Siddaganga Institute of Technology (Affiliated to Visvesvaraya Technological University, Belagavi), Tumakuru 572103, India

3 School of Metallurgy and Materials, University of Birmingham, Edgbaston B15 2TT, UK

4 Department of Chemistry, School of Engineering, Presidency University, Bengaluru 560064, India

bandgap with unaltered tetravalent Ti. With a decrease in the bandgap, intrinsic resistance is found to decrease [15, 16]. Moreover, B-TiO_2 is accompanied by conductive Ti^{3+} and oxygen vacancies. Oxygen vacancies enhance the interlayer spacing, leading to faster Li^+ ions kinetics, and facilitate the reinstitution of host structure during de-/intercalation [17]. Thus, these unique factors make B-TiO_2 an attractive contender as negative electrode for LIBs.

Though it has many salient features, surprisingly it has been a less explored negative electrode for LIBs. Several methods including metal reduction, plasma treatment, high-/low-pressure hydrogen treatment have been proposed to synthesize B-TiO_2 NPs [18–21]. However, these methods demand rigorous reaction conditions. Therefore, a facile and economic synthesis method is highly desirable. Herein, we report the synthesis of B-TiO_2 NPs by simple and scalable sol–gel method followed by calcination at 400 °C in the nitrogen (N_2) atmosphere for 2 h. The obtained B-TiO_2 NPs were characterized with several physicochemical techniques and probed as negative electrode for LIBs.

Experimental section

Titanium (IV) butoxide and thiourea were procured from Sigma-Aldrich. Lauryl lactyl lactate (Koplactylate) surfactant was procured from Kumar Organic Products Pvt. Ltd., India. The chemical reagents were used as received without any purification.

Sol–gel synthesis of B-TiO_2 NPs

B-TiO_2 NPs were synthesized by a simple modified sol–gel method as reported in our earlier work on white TiO_2 [22]. A solution composed of 4 mL of ethanol and 0.9 mL of double-distilled (DD) water was named as A. Another solution B was prepared by mixing 0.5 mL of lauryl lactyl lactate, 8 mL of ethanol, 2 mL of titanium butoxide and 0.1 mL of hydrochloric acid. Solution A was then added to solution B and agitated for 5–8 min until gel was developed. It was allowed to age for 12 h at ambient temperature and then dried at 80 °C for 3 h. The solid gel was transferred and subjected to calcination at 400 °C for 2 h in the tubular furnace under nitrogen (N_2) atmosphere. The obtained compound was black in color.

Material characterization

Powder X-ray diffraction (PXRD) pattern of B-TiO_2 was analyzed using Rigaku SmartLab X-ray diffractometer with monochromatized Cu Kα radiation. The chemical nature of the B-TiO_2 was investigated by X-ray photoelectron spectroscopy (XPS) using Al Kα radiation (1.486 keV, Axis Ultra DLD, Kratos Analytical). Raman spectrum of the sample was recorded using 514.5-nm Ar^+ laser in HORIBA LabRam HR800. Morphological and structural investigations were carried out using scanning electron microscopy (SEM) [FESEM Carl Zeiss (Oxford instrument)] and transmission electron microscopy (TEM) (FEI Tecnai T20 S-TWIN TEM). Quanta Chrome Nova-1000 surface analyzer was used to record surface area and pore size distribution of the sample.

Electrochemical measurements

Coin cells (CR2032, Hohsen Corporation, Japan) were assembled to investigate the electrochemical properties of B-TiO_2 as a negative electrode for LIBs. Lithium (Aldrich) metal was used as both reference and counter electrode. Active material (B-TiO_2), carbon black (Super P, Aldrich) and sodium carboxymethyl cellulose (CMC, Aldrich) were mixed in the weight ratio 85:10:5, and a slurry was prepared in a few drops of *N*-methylpyrrolidinone (NMP, Aldrich). Although CMC is water-soluble, NMP was used to follow the standard practice of electrode formation which tends to avoid water as even PPM level of trapped moisture which can be detrimental to cell performance. The slurry was uniformly coated on a pretreated copper foil before drying it at 110 °C for overnight in a vacuum oven. 1 M $LiPF_6$ dissolved in ethylene carbonate, diethyl carbonate and dimethyl carbonate (2:1:2 v/v) (Chameleon, China) was used as electrolyte, and a porous polypropylene membrane (Celgard 2400) as a separator. The coin cells were fabricated in argon-filled glove box with ~ 1.0 mg cm^{-2} of active material. Cyclic voltammetry, galvanostatic charge–discharge cycling and rate capability measurements were conducted using Biologic Science BCS-8xx series at 22 ± 1 °C. Electrochemical ac impedance spectroscopy was carried out on the cells in the frequency range of 10 mHz to 100 kHz with an amplitude of 10 mV in three-electrode mode.

Results and discussion

The XRD pattern of B-TiO_2 NPs is shown in Fig. 1. All the diffraction peaks in the XRD patterns can be indexed to JCPDS no. 01-073-1764 which corresponds to tetragonal structure of TiO_2. XRD pattern confirms the formation of pure anatase phase as no peaks corresponding to any other polymorphous are present. The XRD pattern also reveals that the B-TiO_2 NPs are crystalline in nature. The average crystallite size of B-TiO_2 is calculated using Debye–Scherrer's equation and found to be ~ 50 nm:

$$D = \frac{0.9\lambda}{\beta \mathrm{Cos}\theta},$$

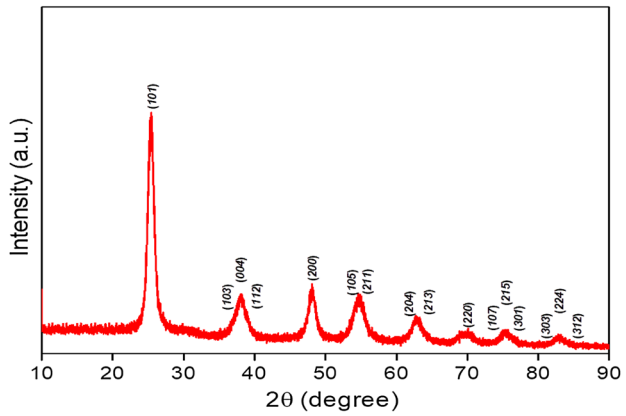

Fig. 1 XRD pattern of the B-TiO_2 NPs

where D is the average crystallite size (nm), λ is the wavelength of Cu Kα (0.154 nm), β is the full width at half maximum (FWHM) in radian, and θ is the Bragg angle. Thus, XRD pattern succeeded in validating the formation of anatase TiO_2 but failed to distinguish between white and black TiO_2.

XPS is a powerful tool to determine and distinguish the contents of a sample. Figure 2 shows the XPS spectra for survey spectrum (A), Ti 2p (B) and O (C). 459.5 (Ti $2p_{3/2}$) and 465.1 (Ti $2p_{1/2}$) eV are the characteristic 2p core level XPS peaks of anatase white TiO_2 (Fig. S1). These peaks correspond to Ti^{4+} in TiO_2, whereas in case of B-TiO_2, a negative shift in binding energy is observed, yielding the centers of the peaks at 458.6 and 464.2 eV. These peaks correspond to the formation of isolated Ti^{3+} defect structure in TiO_2 anatase phase which is stable at room temperature [23–28]. Furthermore, formation of Ti^{3+} is confirmed by convolution of the peaks (Fig. 2b). Annealing the sample at 400 °C in nitrogen flow is accounted for the oxygen vacancies generated in the bulk TiO_{2-x}.

Formation of Ti interstitials and expulsion of oxygen from anion sublattice leaving oxygen vacancies are the chief processes accountable for the formation of high oxygen vacancies in the TiO_{2-x}. Generally, the latter one is extensive than Ti interstitials. The density of carriers, which are regarded as electron donors for TiO_2, is enhanced by the generation of oxygen vacancies. With an increase in donor density in the TiO_{2-x} structure, electrical conductivity increases, whereas bandgap energy decreases, yielding visible active property to the material [23–25]. We can also observe a tiny peak at 400 eV which corresponds to 1s level of nitrogen (Fig. S1). This can be attributed to the presence of chemisorbed nitrogen. Many authors have exposed this contribution and attributed it to molecularly chemisorbed γ-nitrogen [29–34]. Figure 2c shows the XPS spectrum of oxygen. The sample displayed a peak at 529.9 eV which is ascribed to the characteristic peak of Ti–O–Ti [23–28]. The peak is broad and slightly asymmetric, and it may be attributed to Ti–O–N and Ti–O–H. Formation of TiN or TiO_2–TiN mixed phase can be ruled out as XRD pattern does not show any significant impurity peak. Furthermore, no nitrogen precursor has been used in the synthesis. Therefore, asymmetry of oxygen peak is due to bonding of oxygen with chemisorbed nitrogen and hydrogen [29–34]. Thus, XPS spectra reveal the formation Ti^{3+} ions and oxygen vacancies, causing structural defects in TiO_2.

Raman spectroscopy was also carried out on the sample to disclose the formation of B-TiO_2. Figure 3 shows the Raman

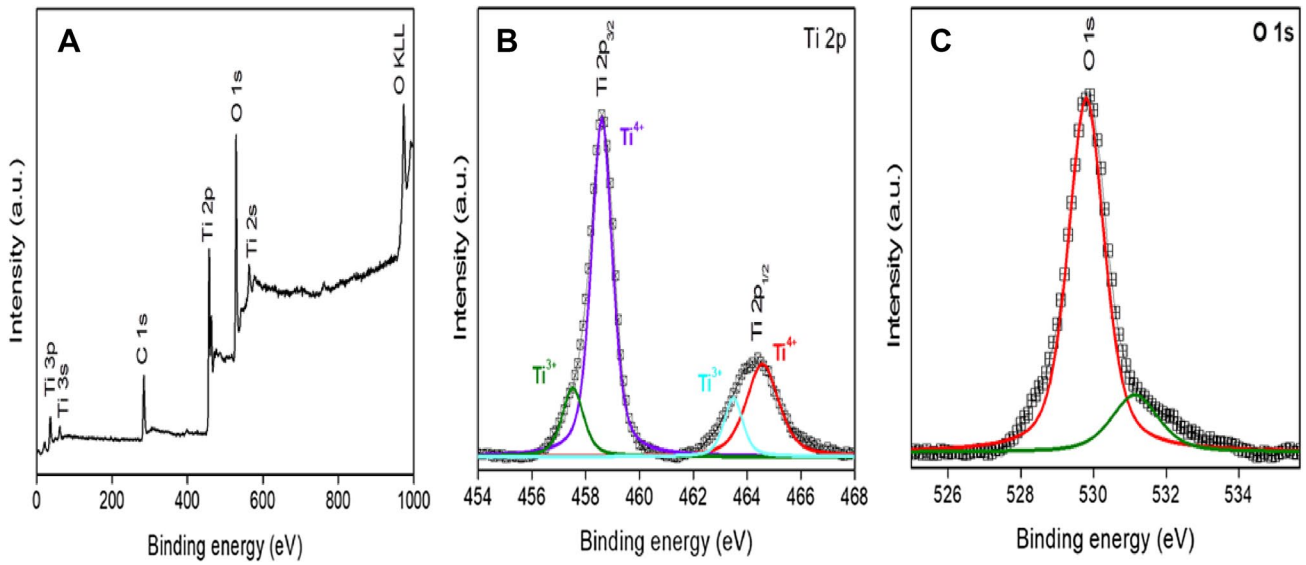

Fig. 2 XPS spectra for survey spectrum (**a**), Ti 2p (**b**) and O 1s (**c**)

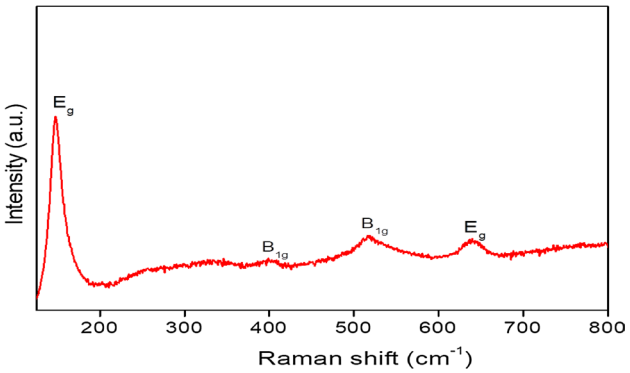

Fig. 3 Raman spectrum of the B-TiO_2

spectrum of B-TiO_2 NPs. The peaks at 147 and 638 cm^{-1} are attributed to E_g modes of vibration. The peaks at 399 and 517 cm^{-1} are ascribed to B_{1g} modes of vibration [35]. The absence of any other peaks represents the purity of the sample. Further, low intensities of the peaks suggest the formation of anatase B-TiO_2 NPs. Morphology of the B-TiO_2 NPs was examined by SEM. Figure 4a, b displays SEM images of B-TiO_2 NPs. SEM images revealed that B-TiO_2 has acquired spongy nature (like partially molten jaggery without much of sharp and clean surface and edges), which is ascribed to the surfactant (lauryl lactyl lactate) used in the synthesis. Lauryl lactyl lactate is an organic compound, which is non-toxic, highly safe, biodegradable, and generally used in the food industries. Among many reagents, lauryl lactyl lactate is implemented in the synthesis of foams. Interestingly, the surfactant effectively participated in the reaction and provided spongy nature to the sample. Figure 4c shows the energy-dispersive X-ray (EDAX) spectrum of B-TiO_2 NPs. The EDAX spectrum reveals the presence of titanium and oxygen.

TEM was carried out to further obtain the insight into the morphology of the B-TiO_2 NPs. Figure 5a, b depicts low-resolution TEM images of B-TiO_2 NPs, which present the dispersion of B-TiO_2 NPs. Figure 5c depicts the high-resolution TEM (HRTEM) image of B-TiO_2 NPs. From the image, defective surface of TiO_2 can be observed confirming the formation of Ti^{3+} ions and oxygen vacancies. Plane and d spacing values calculated from HRTEM image are coherent with XRD results. The size of B-TiO_2 NPs is found to be ~ 10 nm. Figure 5d depicts the selected area electron diffraction (SAED) patterns of B-TiO_2 NPs. The SAED pattern is displayed as concentric circles whose d spacing values are consistent with XRD data. Thus, spongy nature, distracted structure and nanosized particles make B-TiO_2 an attractive candidate as negative electrode for LIBs.

Surface area and porosity of the material are the two critical points which play a significant role in enhancing the capacity storage and stability of the electrode. Nitrogen (N_2) adsorption–desorption measurements were carried out to calculate Brunauer–Emmett–Teller (BET) specific surface area (Fig. 6) and Barrett–Joyner–Halenda (BJH) pore size distribution of B-TiO_2 (Fig. 6, inset). B-TiO_2 exhibits type IV isotherm with hysteresis loop signifying the mesoporous nature of the sample [36]. The BET specific surface area B-TiO_2 is found to be 13 $m^2\ g^{-1}$ with average pore size distribution of 2–3 nm. Since we carried out the annealing at 400 °C, we ended up getting high crystallinity and low surface area with mesoporous nature.

Electrochemical performance

The electrochemical properties of B-TiO_2 were evaluated in coin cell configuration at room temperature. Cyclic voltammetry (CV) was implemented as the primary tool to understand the electrochemical redox reactions during charging and discharging. Figure 7 shows the cyclic voltammogram of B-TiO_2 in the voltage range 0.1–3.0 V obtained at the sweep rate of 0.1 mV s^{-1}. The first cathodic sweep consists of three peaks at 0.65, 1.67 and 2.36 V. The peak at 2.36 V in the first sweep disappears in the subsequent cycles, indicating the formation of irreversible SEI in the first cycle, and this may be due to extension of stability window of electrolyte down

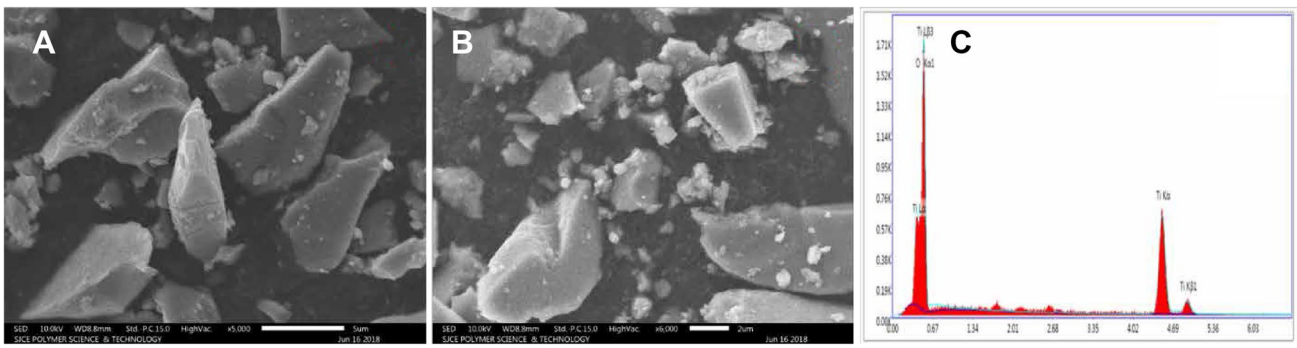

Fig. 4 SEM images (**a**, **b**) and EDAX (**c**) of the B-TiO_2 NPs

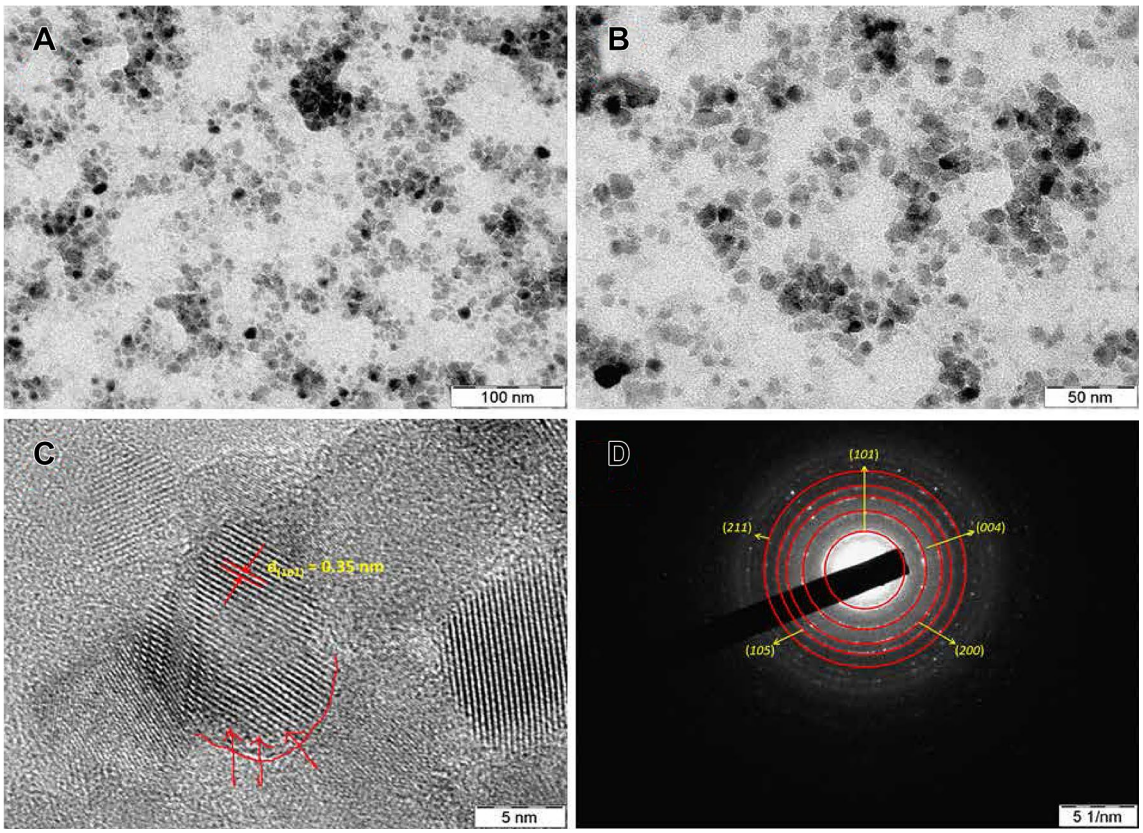

Fig. 5 TEM images (**a**, **b**), HRTEM image (**c**) and SAED patterns (**d**) of the B-TiO_2 NPs

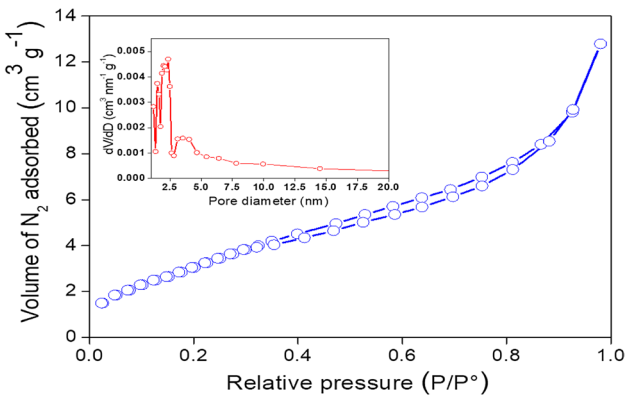

Fig. 6 Nitrogen adsorption–desorption isotherm of B-TiO_2 NPs [inset: pore size distribution]

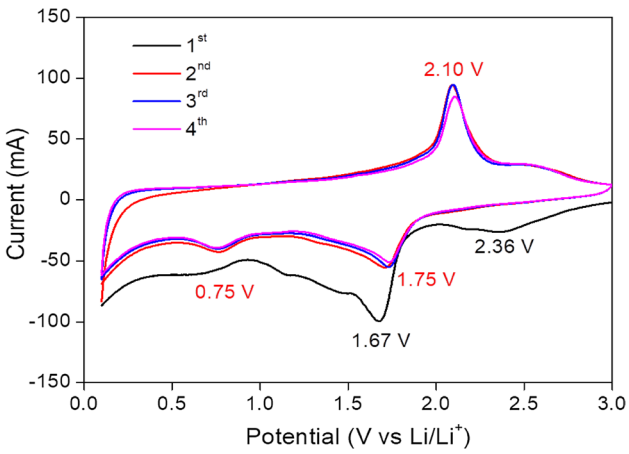

Fig. 7 Cyclic voltammogram of B-TiO_2 NPs

to 0.7–0.8 V vs Li [37–39]. The couple of peaks at 0.65 and 1.67 V in the cathodic sweep are assigned to insertion of lithium into TiO_2 matrix and to the structure transformation from tetragonal TiO_2 to orthorhombic Li_xTiO_2, where x is insertion coefficient. These peaks shift right to 0.75 and 1.75 V in the subsequent cycles, indicating enhanced kinetics after first cycle [10, 12, 40–60]. Insertion mechanism Li^+ into TiO_2 matrix is further discussed later. The anodic peak at 2.10 V corresponds to delithiation from TiO_2 matrix. The overlap of CV curves suggests that the material can uptake and release Li^+ with good reversibility.

Overall electrochemical reaction taking place may be illustrated by the following equation:

$$TiO_2 + xLi^+ + xe^- \longleftrightarrow Li_xTiO_2 \ (0 < x \leq 1)$$

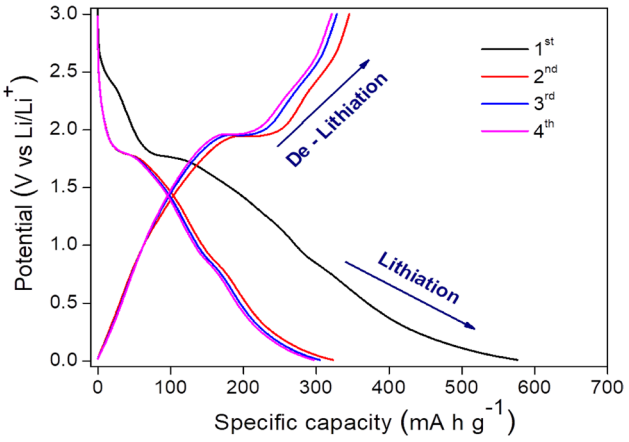

Fig. 8 Galvanostatic charge–discharge profile of B-TiO_2 NPs

Figure 8 shows the galvanostatic charge–discharge profile of B-TiO_2 at 1 C rate (1 C = 335 mA h g^{-1}), in the potential range 0.1–3.0 V. The first lithiation and delithiation capacities were found to be 575 and 345 mA h g^{-1}, respectively. The excess capacity in the first few cycles is attributed to widening of potential range, defective TiO_2 and formation of SEI [39, 57, 61–66]. Vereecken et al. demonstrated an increase in the capacity by ~ 30% when the lower potential barrier was dragged from 1.0 to 0.1 V for TiO_2. The excess capacity was attributed to widening of potential window, i.e., a large potential difference. They also observed sluggish delithiation kinetics for first few cycles, which was ascribed to excess of Li^+ ions present in TiO_2 matrix [61]. Harutyunyana et al. showed that high concentration of defects and edges in the electrode matrix is responsible for excess capacity in first few cycles [62]. Similarly, Schuhmann et al. demonstrated that SEI formed in case of TiO_2 has high Li-ion transport ability and thereby it enhances the cycle stability of TiO_2 [39].

Furthermore, Reddy et al. exclusively carried out electrochemical impedance measurements on TiO_2 during charge and discharge processes at different potentials. Reddy group demonstrated that the resistance will decrease as we move from potential 3.0 to 0.05 V (lithiation). However, resistance in the potential window (1.6–2.1 V) where typical redox reaction takes place will be low compared to impedance at different potentials [67–71]. An irreversible capacity loss is generally observed in the first cycle (here 40%) when TiO_2 is cycled in the wider potential window and is due to (1) sluggish delithiation kinetics for first few cycles, which is due to excess of Li^+ ions trapped in TiO_2 matrix; (2) irreversible intercalation/insertion of Li^+ ions into the matrix; (3) electrolyte decomposition; and (4) formation of SEI [39, 56, 61–66].

The lithium intercalation mechanism can be disintegrated into three parts. Part-1 corresponds to 3.0–1.75 V potential window where voltage drops from OCV to 1.75 V. This range corresponds to intercalation of Li^+ ions into tetragonal TiO_2 matrix without the nucleation of other phases [10, 12, 40–60]. Part-2 corresponds to plateau at ≈ 1.75 V. In the literature, this plateau is ascribed to formation and coexistence of orthorhombic phase along with tetragonal phase [10, 12, 40–60]. Part-3 extends from 1.75 to 0.1 V. Earlier studies have proven that Li^+ insertion in this range depends on the size, morphology and defects of host material [10, 12, 40–60]. Furthermore, it is also illustrated the formation of reversible interfacial lithium storage which holds responsible for excess lithium insertion by means of charge separation [60]. The delithiation curve shows a broad hump at 2.10 V corresponding to removal of Li^+ ions from the B-TiO_2 matrix. The potential profile is in good agreement with CV results. All the results are coherent with earlier reports [9, 35, 36, 72].

Figure 9 shows the cyclic performance and coulombic efficiency of B-TiO_2 over 150 cycles at 1 and 5 C rates. The charge and discharge capacities for second, third and fourth cycles at 1 C were found to be 323 and 327 mA h g^{-1}, 305 and 320 mA h g^{-1}, and 298 and 310 mA h g^{-1}, respectively. After a huge coulombic efficiency (CE) fall in the first cycle, it began to recover from the next cycle, reached about 100% efficiency in the second cycle and remained constant till the end of 150 cycles. At end of 150 cycles, it exhibited charge and discharge capacities of 275 and 283 mA h g^{-1}, respectively. After first five cycles, it displayed excellent stability over 150 cycles by displaying only 0.09% capacity loss per cycle. Furthermore, its cyclic performance was investigated at 5 C to reveal its behavior at high rates. Interestingly, it displayed remarkable stability over 150 cycles by displaying capacity loss of only 0.16% per cycle. On cycling at 5 C rate, the charge and discharge capacities for first three cycles were found to be 508 and 276 mA h g^{-1}, 279 and 260 mA h g^{-1}, and 263 and 254 mA h g^{-1}, respectively. It delivered

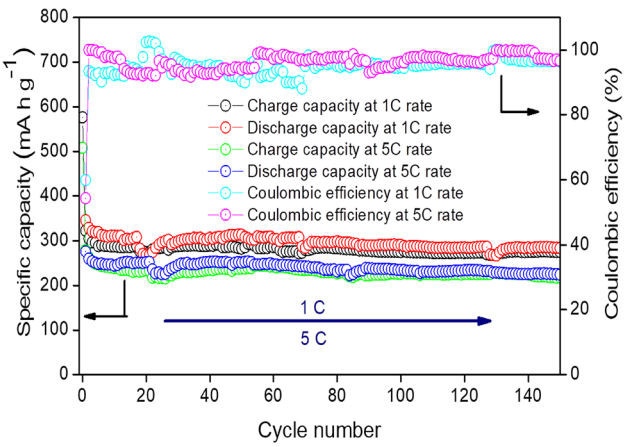

Fig. 9 Cycling performance and coulombic efficiency of B-TiO_2 NPs

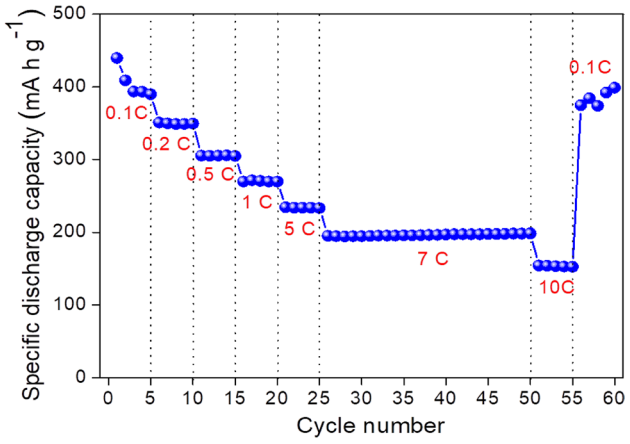

Fig. 10 Rate capability of B-TiO_2 NPs

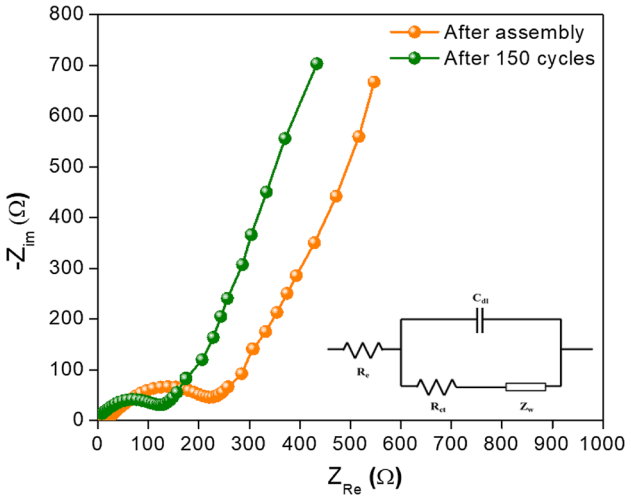

Fig. 11 Nyquist plots of B-TiO_2 NPs after assembly and after 150 cycles

charge and discharge capacities of 220 and 226 mA h g^{-1} at the end of 150 cycles.

The applications of B-TiO_2 for different rates were investigated to understand memory effect. Figure 10 depicts the rate capability of B-TiO_2 at different rates. It exhibited discharge capacities of 394, 350, 307 and 270 mA h g^{-1} at currents rates of 0.1, 0.2, 0.5 and 1 C, respectively. It exhibited excellent stability and high capacity by delivering high discharge capacities of 197 and 153 mA h g^{-1} at very high current rates of 7 and 10 C, respectively. The discharge capacity is restored to 392 mA h g^{-1} when current is reverted to 0.1 C.

The high capacity and excellent stability of the electrode are attributed to the presence of Ti^{3+} ions and oxygen vacancies. As Ti^{3+} ions are highly conductive in nature, TiO_2 with Ti^{3+} ions is promoted as a strong contender for negative electrode in LIBs. Meanwhile, oxygen vacancies formed during the generation of Ti^{3+} ions also favor the lithium storage by providing enhanced interlayer spacing. Thus, Ti^{3+} ions and oxygen vacancies play a significant role in enhanced Li^+ ion storage and excellent stability. It is also worth noting the use of CMC as a binder. The excessive polar functional groups are exploited as excellent chemical bonding agents to bind the active material and current collector together, thereby curtailing the structural destruction during the Li^+ ions de-/intercalation. The excellent electrochemical performance of B-TiO_2 is also benefited from its nanosize, high surface area, mesoporosity and spongy nature of the electrode material.

The electrochemical impedance spectra (EIS) were recorded after assembly and after 150 cycles at 3.00 V (i.e., delithiated state) to analyze the transport kinetics of B-TiO_2 (Fig. 11). The impedance spectrum is represented as Nyquist plots, and it consists of low-frequency linear part and high-frequency semicircles. The diameter of semicircle in Nyquist plot of impedance spectrum is a measure of charge-transfer resistance and SEI layer resistance. The lower-frequency linear spike corresponds to diffusion-limited Warburg element [73, 74]. A lower charge-transfer resistance of 120 Ω is obtained for B-TiO_2 cell after 150 cycles, whereas it displayed a high resistance of 230 Ω after assembly. The declined charge-transfer resistance suggests an increase in the kinetics of electron-transfer reaction with cycling.

Conclusion

Black TiO_2 NPs were synthesized by a simple surfactant-assisted sol–gel method. The formation of Ti^{3+} ions and oxygen vacancies were ascertained by XPS studies and were found to be responsible for the formation of black-colored defective TiO_2. The synthesized defective B-TiO_2 NPs were probed as negative electrode for LIBs. It exhibited discharge capacities of 275 and 220 mA h g^{-1} at very high current rates of 1 C and 5 C, respectively, even after 100 cycles of charge and discharge. The high specific capacity and excellent stability of B-TiO_2 NPs are attributed to the formation of Ti^{3+} ions and oxygen vacancies. As Ti^{3+} ions are highly conductive in nature, they enhance the lithium kinetics. The oxygen vacancies which are formed during the generation of Ti^{3+} ions also favor the lithium storage by providing enhanced interlayer spacing. These are the driving forces for us to implement and investigate B-TiO_2 as negative electrode for LIBs. Thus, it is reckoned that defective B-TiO_2 can serve as a potential negative electrode for LIBs.

Acknowledgements SBP and GN greatly thank BRNS-BARC, DAE (No. 37(2)/14/25/2015/BRNS), Bombay, Govt. of India, for financial sponsorship. Thanks are due to CoE—TEQIP, Director and Principal, Siddaganga Institute of Technology (SIT), Tumakuru, for constant support and encouragement. Thanks to Prof. N. Munichandraiah, Dept. of

Inorganic and Physical Chemistry, Indian Institute of Science, Bangalore, for providing glove box facility to assemble the cells.

Compliance with ethical standards

Conflict of interest The authors declare no competing financial interest.

References

1. Liu, J., Tang, S., Lu, Y., Cai, G., Liang, S., Wang, W., Chen, X.: Synthesis of Mo_2N nanolayer coated MoO_2 hollow nanostructures as high-performance anode materials for lithium-ion batteries. Energy Environ. Sci. **6**, 2691–2697 (2013)
2. Islam, M., Ali, G., Jeong, M.G., Choi, W.C., Chung, K.Y., Jung, H.G.: Study on the electrochemical reaction mechanism of $NiFe_2O_4$ as a high-performance anode for li-ion batteries. ACS Appl. Mater. Interfaces. **9**, 14833–14843 (2017)
3. Patil, S.B., Raghu, M.S., Kishore, B., Nagaraju, G.: Enhanced electrochemical performance of few-layered MoS_2-rGO nanocomposite for lithium storage application. J. Mater. Sci. Mater. Electr. (2018). https://doi.org/10.1007/s10854-018-0295-3
4. Patil, S.B., Kishore, B., Nagaraj, M.K., Nagaraju, G., Velu, U.: Mesoporous $MnMoO_4$ nanorods for enhanced electrochemical performance. ChemistrySelect **3**, 7490–7495 (2018)
5. Armstrong, A.R., Armstrong, G., Canales, J., Bruce, P.G.: Angew. TiO_2-B nanowires. Chem. Int. Ed. **43**, 2286–2288 (2004)
6. Armstrong, A.R., Armstrong, G., Canales, J., Garcia, R., Bruce, P.G.: Lithium ion intercalation into TiO_2-B nanowires. Adv. Mater. **17**, 862–865 (2005)
7. Ryu, W.H., Nam, D.H., Ko, Y.S., Kim, R.H., Kwon, H.S.: Electrochemical performance of a smooth and highly ordered TiO_2 nanotube electrode for li-ion batteries. Electrochim. Acta **61**, 19–24 (2012)
8. Naldoni, A., Allieta, M., Santangelo, S., Marelli, M., Fabbri, F., Cappelli, S., Bianchi, C.L., Psaro, R., Dal Santo, V.: Effect of nature and location of defects on bandgap narrowing of black TiO_2 nanoparticles. J. Am. Chem. Soc. **134**, 7600–7603 (2012)
9. Eom, J.Y., Lim, S.J., Lee, S.M., Ryu, W.H., Kwon, H.S.: Black titanium oxide nanoarray electrodes for high rate li-ion microbatteries. J. Mater. Chem. A **3**, 11183–11188 (2015)
10. Wagemaker, M., Kentgens, A.P.M., Mulder, F.M.: Equilibrium lithium transport between nanocrystalline phases in intercalated TiO_2 anatase. Nature **418**, 397–399 (2002)
11. Hu, Y.-S., Kienel, L., Guo, Y.-G., Maier, J.: High lithium electroactivity of nanometer-sized rutile-TiO_2. Adv. Mater. **18**, 1421–1426 (2006)
12. Sudant, G., Baudrin, E., Larcher, D., Tarascon, J.-M.: Electrochemical lithium reactivity with nanotextured anatase-type TiO_2. J. Mater. Chem. **15**, 1263–1269 (2005)
13. Cheng, X.L., Hu, M., Huang, R., Jiang, J.S.: HF-free synthesis of anatase TiO_2 nanosheets with largely exposed and clean 001 facets and their enhanced rate performance as anodes of lithium ion battery. ACS Appl. Mater. Interfaces. **6**, 19176–19183 (2014)
14. Liu, H., Li, W., Shen, D., Zhao, D., Wang, G.: Graphite carbon conformal coating of mesoporous TiO_2 hollow spheres for high-performance lithium ion battery anodes. J. Am. Chem. Soc. **137**, 13161–13166 (2015)
15. Hu, Y.H.: A highly efficient photocatalyst—hydrogenated black TiO_2 for the photocatalytic splitting of water. Angew. Chem. **51**, 12410–12412 (2012)
16. Nowotny, M.K., Bak, T., Nowotny, J.: Electrical properties and defect chemistry of TiO_2 single crystal. I. Electrical conductivity. J. Phys. Chem. B **110**, 16270–16282 (2006)
17. Kim, H.S., Cook, J.B., Lin, H., Ko, J.S., Tolbert, S.H., Ozolins, V., Dunn, B.: Oxygen vacancies enhance pseudocapacitive charge storage properties of MoO_{3-x}. Nat. Mater. **16**, 454–460 (2017)
18. Ullattil, S.G., Narendranath, S.B., Pillai, S.C., Periyat, P.: Black TiO_2 nanomaterials: a review of recent advances. Chem. Eng. J. **343**, 708–736 (2018)
19. Ma, Y., Wang, X., Jia, Y., Chen, X., Han, H., Li, C.: Titanium dioxide-based nanomaterials for photocatalytic fuel generations. Chem. Rev. **114**, 9987–10043 (2014)
20. Chen, X., Liu, L., Huang, F.: Black titanium dioxide (TiO_2) nanomaterials. Chem. Soc. Rev. **44**, 1861–1885 (2015)
21. Kapilashrami, M., Zhang, Y., Liu, Y.-S., Hagfeldt, A., Guo, J.: Probing the optical property and electronic structure of TiO_2 nanomaterials for renewable energy applications. Chem. Rev. **114**, 9662–9707 (2014)
22. Phattepur, H., Siddaiah, G.B., Nagaraju, G.: Synthesis and characterisation of mesoporous TiO_2 nanoparticles by novel surfactant assisted sol–gel method for the degradation of organic compounds. Periodica Polytech. Chem. Eng. **63**, 85–95 (2019)
23. Cui, H.L., Zhao, W., Yang, C.Y., Yin, H., Lin, T.Q., Shan, Y.F., Xie, Y., Gu, H., Huang, F.Q.: Black TiO_2 nanotube arrays for high-efficiency photoelectrochemical water-splitting. J. Mater. Chem. A **2**, 8612–8616 (2014)
24. Chen, X.B., Liu, L., Liu, Z., Marcus, M.A., Wang, W.C., Oyler, N.A., Grass, M.E., Mao, B.H., Glans, P.A., Yu, P.Y., Guo, J.H., Mao, S.S.: Properties of disorder-engineered black titanium dioxide nanoparticles through hydrogenation. Sci. Rep. **3**, 1510–1517 (2013)
25. Ryu, W.H., Lee, Y.W., Nam, Y.S., Youn, D.Y., Park, C.B., Kim, I.D.: Crystalline IrO_2-decorated TiO_2 nanofiber scaffolds for robust and sustainable solar water oxidation. J. Mater. Chem. A **2**, 5610–5615 (2014)
26. Liu, D.W., Zhang, Y.H., Xiao, P., Garcia, B.B., Zhang, Q.F., Zhou, X.Y., Jeong, Y.H., Cao, G.Z.: TiO_2 nanotube arrays annealed in CO exhibiting high performance for lithium ion intercalation. Electrochim. Acta **54**, 6816–6820 (2009)
27. Wang, G.M., Wang, H.Y., Ling, Y.C., Tang, Y.C., Yang, X.Y., Fitzmorris, R.C., Wang, C.C., Zhang, J.Z., Li, Y.: Hydrogen-treated TiO_2 nanowire arrays for photoelectrochemical water splitting. Nano Lett. **11**, 3026–3033 (2011)
28. Lu, X.H., Wang, G.M., Zhai, T., Yu, M.H., Gan, J.Y., Tong, Y.X., Li, Y.: Hydrogenated TiO_2 nanotube arrays for supercapacitors. Nano Lett. **12**, 1690–1696 (2012)
29. Jagadale, T.C., Takale, S.P., Sonawane, R.S., Joshi, H.M., Patil, S.I., Kale, B.B., Ogale, S.B.: *N*-Doped TiO_2 nanoparticle based visible light photocatalyst by modified peroxide sol–gel method. J. Phys. Chem. C **112**, 14595–14602 (2008)
30. Asahi, R., Morikawa, T., Ohwaki, T., Aoki, K., Taga, Y.: Visible-light photocatalysis in nitrogen-doped titanium oxides. Science **293**, 269–271 (2001)
31. Chen, C., Bai, H., Chang, C.: Effect of plasma processing gas composition on the nitrogen doping status and visible light photocatalysis of TiO_2. J. Phys. Chem. C **111**(15228), 15235 (2007)

32. Saha, N.C., Tompkins, H.G.: Titanium nitride oxidation chemistry: an X-ray photoelectron spectroscopy study. J. Appl. Phys. **72**, 3072 (1992)
33. Glaser, A., Surnev, S., Netzer, F.P., Fateh, N., Fontalvo, G.A., Mitterer, C.: Oxidation of vanadium nitride and titanium nitride coatings. Surf. Sci. **601**, 1153–1159 (2007)
34. Gopinath, C.S.: Comment on "Photoelectron spectroscopic investigation of nitrogen-doped titania nanoparticles". J. Phys. Chem. B **110**, 7079–7080 (2006)
35. Myung, S.T., Kikuchi, M., Yoon, C.S., Yashiro, H., Kim, S.J., Sun, Y.K., Scrosati, B.: Black anatase titania enabling ultra high cycling rates for rechargeable lithium batteries. Energy Environ. Sci. **6**, 2609–2614 (2013)
36. Sunkara, S., Munichandraiah, N., Varma, K.B.R., Shivashankar, S.A.: A sonochemical approach for the synthesis of thermally stable mesoporous microspheres of TiO_2 for use as high performance anodes for li-ion batteries. New J. Chem. **40**, 7197–7203 (2016)
37. Madej, E., Ventosa, E., Klink, S., Schuhmann, W., La Mantia, F.: Aging effects of anatase TiO_2 nanoparticles in Li-ion batteries. Phys. Chem. Chem. Phys. **16**, 7939–7945 (2014)
38. Nan, Y., Li, S., Li, B., Yang, S.: An artificial TiO_2/lithium n-butoxide hybrid SEI layer with facilitated lithium-ion transportation ability for stable lithium anodes. Nanoscale **11**, 2194–2201 (2019)
39. Ventosa, E., Madej, E., Zampardi, G., Mei, B., Weide, P., Antoni, H., Mantia, F.L., Muhler, M., Schuhmann, W.: Solid electrolyte interphase (SEI) at TiO_2 electrodes in li-ion batteries: defining apparent and effective SEI based on evidence from X-ray photoemission spectroscopy and scanning electrochemical microscopy. ACS Appl. Mater. Interfaces. **9**, 3123–3130 (2017)
40. Wagemaker, M., van de Krol, R., Kentgens, A.P.M., van Well, A.A., Mulder, F.M.: Two phase morphology limits lithium diffusion in TiO_2 (anatase): a Li-7 MAS NMR study. J. Am. Chem. Soc. **123**, 11454–11461 (2001)
41. Leroux, F., Dewar, P.J., Intissar, M., Ouvrard, G., Nazar, L.F.: Study of the formation of mesoporous titania via a template approach and of subsequent Li insertion. J. Mater. Chem. **12**, 3245–3253 (2002)
42. Maier, J.: Defect chemistry and ion transport in nanostructured materials—Part, II. Aspects of nanoionics. Solid State Ionics **157**, 327–334 (2003)
43. Wagemaker, M., Kearley, G.J., van Well, A.A., Mutka, H., Mulder, F.M.: Multiple li positions inside oxygen octahedra in lithiated TiO_2 anatase. J. Am. Chem. Soc. **125**, 840–848 (2003)
44. Wagemaker, M., Lutzenkirchen-Hecht, D., van Well, A.A., Frahm, R.: Atomic and electronic bulk versus surface structure: lithium intercalation in anatase TiO_2. J. Phys. Chem. B **108**, 12456–12464 (2004)
45. Wagemaker, M., Borghols, W.J.H., Eck, E.R.H., Kentgens, A.P.M., Kearley, G.J., Mulder, F.M.: The influence of size on phase morphology and Li-ion mobility in nano-sized lithiated anatase TiO_2. Chem.-Eur. J. **13**, 2023–2028 (2007)
46. Wagemaker, M., Simon, D.R., Kelder, E.M., Schoonman, J., Ringpfeil, C., Haake, U., Lutzenkirchen-Hecht, D., Frahm, R., Mulder, F.M.: A kinetic two-phase and equilibrium solid solution in spinel $Li_{4+x}Ti_5O_{12}$. Adv. Mater. **18**, 3169–3173 (2006)
47. Wagemaker, M., Borghols, W.J.H., Mulder, F.M.: Large impact of particle size on insertion reactions. A case for anatase Li_xTiO_2. J. Am. Chem. Soc. **129**, 4323–4327 (2007)
48. Dambournet, D., Belharouak, I., Amine, K.: Tailored preparation methods of TiO_2 anatase, rutile, brookite: mechanism of formation and electrochemical properties. Chem. Mater. **22**, 1173–1179 (2010)
49. Pol, V.G., Kang, S.-H., Calderon-Moreno, J.M., Johnson, C.S., Thackeray, M.M.: Autogenic reactions for preparing carbon-encapsulated, nanoparticulate TiO_2 electrodes for lithium-ion batteries. J. Power Sources **195**, 5039–5043 (2010)
50. Shin, J.-Y., Samuelis, D., Maier, J.: Sustained lithium-storage performance of hierarchical, nanoporous anatase TiO_2 at high rates: emphasis on interfacial storage phenomena. Adv. Funct. Mater. **21**, 3464–3472 (2011)
51. Ortiz, G.F., Hanzu, I., Djenizian, T., Lavela, P., Tirado, J.L., Knauth, P.: Alternative li-ion battery electrode based on self-organized titania nanotubes. Chem. Mater. **21**, 63–67 (2009)
52. Beuvier, T., Richard-Plouet, M., Mancini-Le Granvalet, M., Brousse, T., Crosnier, O., Brohan, L.: TiO_2(B) nanoribbons as negative electrode material for lithium ion batteries with high rate performance. Inorg. Chem. **49**, 8457–8464 (2010)
53. Kavan, L.: Electrochemistry of titanium dioxide: some aspects and highlights. Chem. Rec. **12**, 131–142 (2012)
54. Froschl, T., Hörmann, U., Kubiak, P., Kucerova, G., Pfanzelt, M., Weiss, C.K., Behm, R.J., Husing, N., Kaiser, U., Landfester, K., Wohlfahrt-Mehrens, M.: High surface area crystalline titanium dioxide: potential and limits in electrochemical energy storage and catalysis. Chem. Soc. Rev. **41**, 5313–5360 (2012)
55. Berger, T., Monllor-Satoca, D., Jankulovska, M., Lana-Villarreal, T., Gomez, R.: The electrochemistry of nanostructured titanium dioxide electrodes. Chem. Phys. Chem. **13**, 2824–2877 (2012)
56. Borghols, W.J.H., Wagemaker, M., Lafont, U., Kelder, E.M., Mulder, F.M.: Size effects in the $Li_{4+x}Ti_5O_{12}$ spinel. J. Am. Chem. Soc. **131**, 17786–17792 (2009)
57. Borghols, W.J.H., Lutzenkirchen-Hecht, D., Haake, U., Chan, W., Lafont, U., Kelder, E.M., van Eck, E.R.H., Kentgens, A.P.M., Mulder, F., Wagemaker, M.: Lithium storage in amorphous TiO_2 nanoparticles. J. Electrochem. Soc. **157**, A582–A588 (2010)
58. Ren, Y., Hardwick, L.J., Bruce, P.G.: Lithium intercalation into mesoporous anatase with an ordered 3D pore structure. Angew. Chem. Int. Ed. **49**, 2570–2574 (2010)
59. Guo, Y.-G., Hu, Y.-S., Maier, J.: Synthesis of hierarchically mesoporous anatase spheres and their application in lithium batteries. Chem. Commun. (2006). https://doi.org/10.1039/b605090e
60. Gentili, V., Brutti, S., Hardwick, L.J., Armstrong, A.R., Panero, S., Bruce, P.G.: Lithium insertion into anatase nanotubes. Chem. Mater. **22**, 4468–4476 (2012)
61. Moitzheim, S., De Gendt, S., Vereecken, P.M.: Investigation of the li-ion insertion mechanism for amorphous and anatase TiO_2 thin-films. J. Electrochem. Soc. **166**, 1–9 (2019)
62. Omichi, K., Ramos-Sanchez, G., Rao, R., Pierce, N., Chen, G., Balbuena, P.B., Harutyunyana, A.R.: Origin of excess irreversible capacity in lithium-ion batteries based on carbon nanostructures. J. Electrochem. Soc. **162**, A2106–A2115 (2015)
63. Madian, M., Eychmuller, A., Giebeler, L.: Current advances in TiO_2-based nanostructure electrodes for high performance lithium ion batteries. Batteries **4**, 7–43 (2018)
64. Lee, K.H., Song, S.W.: One-step hydrothermal synthesis of mesoporous anatase TiO_2 microsphere and interfacial control for enhanced lithium storage performance. ACS Appl. Mater. Interfaces. **3**, 3697–3703 (2011)
65. Yeh, H.L., Tai, S.H., Hsieh, C.M., Chang, B.K.: First-principles study of lithium intercalation and diffusion in oxygen-defective titanium dioxide. J. Phys. Chem. C **122**, 19447–19454 (2018)
66. Wang, J., Polleux, J., Lim, J., Dunn, B.: Pseudocapacitive contributions to electrochemical energy storage in TiO_2 (anatase) nanoparticles. J. Phys. Chem. C **111**, 14925–14931 (2007)
67. Cherian, C.T., Reddy, M.V., Magdaleno, T., Sow, C.H., Ramanujachary, K.V., Subba Rao, G.V., Chowdari, B.V.R.: (N, F)-Co-doped TiO2: synthesis, anatase-rutile conversion and li-cycling properties. Cryst. Eng. Comm **14**, 978–986 (2012)

68. Reddy, M.V., Aloysius Chan, T.Y., Adams, S.: Effect of molten salt synthesis temperature on TiO_2 and li cycling properties. J. Solid State Electrochem. **22**, 429–439 (2018)
69. Reddy, M.V., Madhavi, S., Subba Rao, G.V., Chowdari, B.V.R.: Metal oxyfluorides $TiOF_2$ and NbO_2F as anodes for li-ion batteries. J. Power Sour. **162**, 1312–1321 (2006)
70. Reddy, M.V., Jose, R., Teng, T.H., Chowdari, B.V.R., Ramakrishna, S.: Preparation and electrochemical studies of electrospun TiO_2 nanofibers and molten salt method nanoparticles. Electrochim. Acta **55**, 3109–3117 (2010)
71. Reddy, M.V., Sharma, N., Adams, S., Rao, R.P., Peterson, V.K., Chowdari, B.V.R.: Evaluation of undoped and M-doped TiO_2, where M = Sn, Fe, Ni/Nb, Zr, V, and Mn, for lithium-ion battery applications prepared by the molten-salt method. RSC Adv. **5**, 29535–29544 (2015)
72. Yan, X., Wang, Z., He, M., Hou, Z., Xia, T., Liu, G., Chen, X.: TiO_2 nanomaterials as anode materials for lithium-ion rechargeable batteries. Energy Technol. **3**, 801–814 (2015)
73. Patil, S.B., Kishore, B., Nagaraju, G., Dupont, J.: High capacity MoO_3/rGO nanocomposite anode for lithium ion batteries: an intuition into the conversion mechanism of MoO_3. New J. Chem. **42**, 18569–18577 (2018)
74. Patil, S.B., Kishore, B., Reddy, V., Nagaraju, G.: Composition of MoO_2 nanoparticles with RGO sheets as improved lithium ion battery anode. Chem. Select **3**, 13289–13296 (2018)